Recent results related to excited states of 6Be and 10He

EPJ Web of Conferences **38**, 15002 (2012)
DOI: 10.1051/epjconf/20123815002

Recent results related to excited states of ^{6}Be and ^{10}He

A. S. Fomichev[1], A. A. Bezbakh[1], V. Chudoba[1,2], I. A. Egorova[3], S. N. Ershov[3], M. S. Golovkov[1], A. V. Gorshkov[1], L. V. Grigorenko[1,4,5], P. Jaluvkova[1,2], G. Kaminski[1,6], S. A. Krupko[1], E. A. Kuzmin[5], E. Yu. Nikolskii[5,7], I. G. Mukha[4], Yu. L. Parfenova[1], P. G. Sharov[1], S. I. Sidorchuk[1], R. S. Slepnev[1], S. V. Stepantsov[1], G. M. Ter-Akopian[1], R. Wolski[1,6], M. V. Zhukov[8], A. A. Yukhimchuk[9], S. V. Filchagin[9], A. A. Kirdyashkin[9], I. P. Maksimkin[9], and O. P. Vikhlyantsev[9]

[1]Flerov Laboratory of Nuclear Reactions, JINR, Dubna, 141980, Russia
[2]Institute of Physics, Silesian University in Opava, Bezrucovo nam. 13, 74601, Czech Republic
[3]Bogoliubov Laboratory of Theoretical Physics, JINR, Dubna, 141980, Russia
[4]GSI Helmholtzzentrum für Schwerionenforschung, Planckstrasse 1, D-64291 Darmstadt, Germany
[5]Russian Research Center "The Kurchatov Institute", Kurchatov sq. 1, 123182 Moscow, Russia
[6]Institute of Nuclear Physics PAN, Radzikowskiego 152, PL-31342 Krakow, Poland
[7]RIKEN Nishina Center, Hirosawa 2-1, Wako, Saitama 351-0198, Japan
[8]Fundamental Physics, Chalmers University of Technology, S-41296 Göteborg, Sweden
[9]All-Russian Research Institute of Experimental Physics, RU-607190 Sarov, Russia

Abstract. The ^{1}H(^{6}Li,^{6}Be)n charge-exchange reaction and the ^{3}H(^{8}He,p)^{10}He two-neutron transfer reaction were recently carried out at the ACCULINNA fragment separator (FLNR, Dubna) to populate the ground and excited states of ^{6}Be and ^{10}He nuclei, respectively. The ^{6}Be E_T spectrum (E_T is the ^{6}Be energy above its ^{4}He+p+p decay threshold) was obtained with high statistics and described by the well-known 0^+ ground state of ^{6}Be at E_T = 1.37 MeV, the 2^+ state at E_T = 3.05 MeV and a broad structure extending from 4 to 16 MeV which could be interpreted as the isovector soft dipole mode associated with the ^{6}Li ground state. In the ^{10}He case the 0^+ ground state was found at about 2.1(2) MeV ($\Gamma \sim 2$ MeV) above the ^{8}He+n+n breakup threshold. Angular correlations observed for ^{10}He decay products show prominent interference patterns allowing to draw conclusions about the structure of low-energy excited states: 1^- ($E_T \sim 5$ MeV) and 2^+ ($E_T > 6$ MeV).

1 Introduction

There are several issues causing the interest to ^{6}Be and ^{10}He systems [1,2]. The ground state (g.s.) of ^{6}Be is particle unstable. This nucleus is the lightest *true* two-proton (2p) emitter. The true 2p emission is a genuine quantum mechanical effect: a pairing can cause energy conditions in unbound even systems which make emission of one proton impossible, while two protons should be emitted simultaneously. These specific correlations in the decay of ^{6}Be inspired the concept of *democratic decay* [3], which has now become generally accepted. In heavier two-proton unstable nuclei a true 2p emission is arising in the form of the *two proton radioactivity* [4]. Comparative studies of correlations in ^{6}Be versus ^{45}Fe presenting this short-living system in the context of 2p radioactivity investigations are performed in [5]. The ^{6}Be nucleus is the isobaric partner of the ^{6}He nucleus, which is a classical halo nucleus. Enormous effort has been invested in the recent two decades in the studies of the ^{6}He halo structure. Recently it has been demonstrated in Ref. [6] that a valuable alternative to studies of the ^{6}He g.s. itself could be precision studies of the correlations in the decay of the particle unstable ^{6}Be ground state.

In accordance with a conventional shell model ^{10}He is expected to be a double magic nucleus. However, after long searches for nucleon stable ^{10}He it was discovered as a resonance [7-10], but the question about energies, widths and spin-parities of its low-lying states is still open. This could have an impact on theory judgment about the nuclear matter properties, nuclear equation of state and astrophysical nucleosynthesis paths. The last but not the least point is the interest to studies of ^{8}He+n+n correlations from the ^{10}He decay. The instability of the two ^{10}He subsystems causes its "true", i.e. instantaneous, three-body decay into ^{8}He+n+n continuum. In nuclear physics this class of decays remains not fully understood. The ^{10}He case is one where the ascertainment of details of such a decay will be an important step for this exciting subject.

2 Experimental method and results

Both systems were studied with the ACCULINNA fragment separator at U-400M cyclotron (JINR, Dubna)

[11] and under similar experimental conditions: (i) having a cryogenic gas target, (ii) measuring the decay products in the full angular range for the center-of-mass (c.m.) system θ_{cm}=0°–180° and (iii) providing precise energy-angle correlations between the fragments [1,2].

In the ^{6}Be run the primary ^{6}Li beam with the energy of 47 MeV/u was transported by the ACCULINNA to a reaction chamber and was focused on a cryogenic hydrogen target. The energy in the middle of the target was 32.5 MeV/u, an energy spread of 0.5 % and an average beam intensity of ~3 × 10^{7} s^{-1}. The cryogenic cell was 4 mm thick, enclosed with 20 mm diameter, 6 μm thick stainless steel windows. Working pressure and temperature were 3 bar and 35 K, respectively. Reaction products were measured by two identical annular telescopes placed at 9 and 30 cm downstream the target. Each telescope consisted of two position-sensitive silicon detectors (300 and 1000 μm thick) and a set of 16 trapezoid CsI(Tl) crystals with PIN-diode readout. The inner and outer diameters of the active zone for silicon detectors were 32 and 82 mm. The first detector was segmented in 32 rings on one side and 32 sectors on the other. The second silicon detector was segmented in 16 sectors. The CsI(Tl) crystals were 19 mm thick with the inner and outer diameters of the assembly of 37 and 90 mm. Angular ranges of the telescopes were ~3°–8° and ~10°–20°, respectively. Each segment of the telescopes had an independent acquisition line, which allowed a registration of coincidence events caused by several simultaneous detector hits. Particle identification was provided by the standard ΔE-E method.

For the ^{10}He case a primary ^{11}B beam with the energy 36 MeV/u, being delivered by the U-400M cyclotron at extremely high intensity ~5 pμA, bombarded a water-cooled, rotating production target (Be disk 1.8 mm thick and 86 mm in diameter). The secondary 21.5 MeV/u beam of ^{8}He with intensity of ~1.5 × 10^{4} s^{-1} produced at the fragment-separator ACCULINNA hits a cryogenic gas tritium target [6]. Two thin plastic scintillators set on a 8 m base before the tritium target allowed the beam particle identification and the time-of-flight measurement with an accuracy of about 0.5 ns. Two multiwire proportional chambers performed the tracking for incoming ^{8}He ions providing hit positions on the target cell with an accuracy of ~1.5 mm. The target windows of 25 mm in diameter were sealed with two pairs of 8.4 μm stainless steel foils. The 6 mm thick target cell was filled with tritium gas (enriched to 99.7 %) at a pressure of 0.93 bar and cooled down to 26 K. A total integral flux of ^{8}He was ~1.4 × 10^{10}. The concept of the experiment was similar to that applied in our works [10]. This approach implied a detection of recoil protons emitted from the target in a backward direction in a lab system. Such a low-background kinematical range corresponds to small angles in the c.m. system. The protons were detected by a 1 mm thick annular Si detector with the inner and outer diameters of its sensitive area of 32 and 82 mm. Two detector sides were segmented in 16 rings and 16 sectors. The detector was installed 10 cm upstream the target. A telescope composed of six square, 1 mm thick, 61 × 61 mm^2 Si detectors (with 16 strips each) was placed 25 cm downstream the target to detect the ^{8}He fragments originating from the ^{10}He decay in the coincidence with recoil protons. The missing mass spectrum of ^{10}He was measured with a resolution of ~ 0.5 MeV (FWHM) estimated by the Monte-Carlo simulation and found to be in a good agreement with the results obtained in the ^{3}H(^{6}He,p)^{8}He reaction populating the well known 0^{+} and 2^{+} states of ^{8}He.

2.1 ^{6}Be data analysis

The data analysis deals only with those events which correspond to triple p+p+α coincidences. The invariant-mass spectrum of ^{6}Be was reconstructed together with a momentum of c.m. motion of ^{6}Be in the lab system. Due to inverse kinematics for the ^{1}H(^{6}Li,^{6}Be)n reaction, the ^{6}Be decay products flied out in a narrow angular cone relative to the beam direction. Therefore, the experimental setup allowed the registration of ^{6}Be decays almost in whole angular range up to 16 MeV of the ^{6}Be excitation energy with a reasonable efficiency.

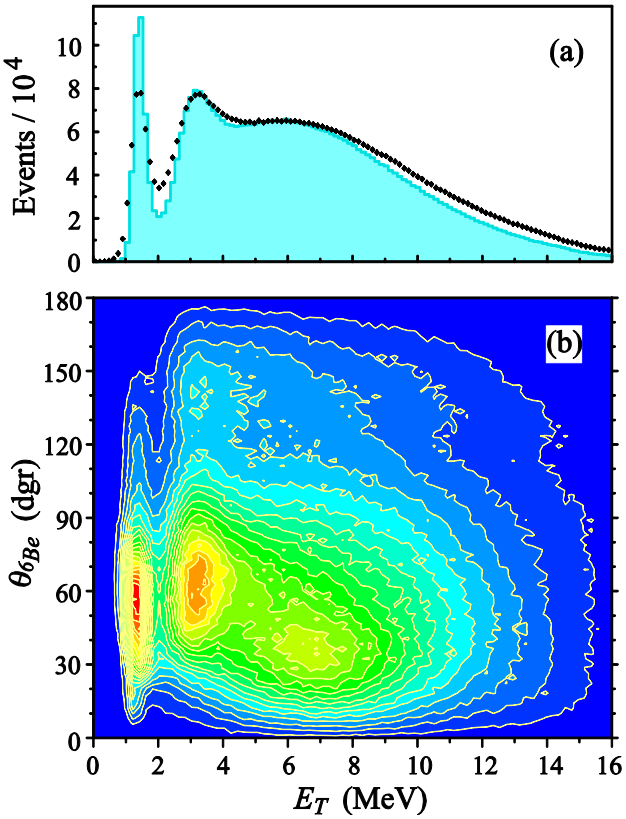

Fig. 1. (a) Experimental energy spectrum E_T of ^{6}Be (points) in comparison with Monte-Carlo simulations (cyan histogram). (b) Contour plot of the measured spectrum E_T versus the θ_{6Be} angle.

In figure 1(a) the ^{6}Be invariant-mass spectrum measured in the whole angular range is presented. The 0^{+} g.s. at E_T = 1.37 MeV and the 2^{+} first excited state at E_T = 3.05 MeV are undoubtedly identified directly in the inclusive spectrum. The width of the g.s. peak demonstrates the overall instrumental energy resolution of the experiment. In the measured spectrum, these two peaks are superimposed on broad hump which starts practically from the energy of the ground state and has a

maximum at E_T ~ 6–7 MeV. The right-hand slope of the hump is due to the decrease of the registration efficiency which is governed by two main factors: (i) the upper limit of the angular acceptance (the ^{6}Be decay products fly out in a wider cone) and (ii) the upper energy threshold of the proton registration (with the increase of the excitation energy the proton energy distribution becomes broader and protons with energy more than 50 MeV are not detected by the first 300 μm detector). In figure 1(b), the ^{6}Be invariant mass spectrum is shown as a two dimensional plot E_T versus θ_{6Be} where θ_{6Be} is the ^{6}Be c.m. angle for the ^{1}H(^{6}Li,^{6}Be)n reaction. It should be noted that the broad hump is characterized by a regular behavior in the whole angular range. Moreover this structure exhibits similar regularities both in angular distribution and in distributions of kinematical variables for three-body decay.

The ^{6}Be ground state population in a charge-exchange reaction corresponds mainly to the $\Delta L = 0$ orbital angular momentum transfer, providing a maximum of the cross section at zero degree. In the experimental spectrum shown in figure 1(b), this maximum is suppressed by the low efficiency due to a central hole of the first telescope. The central hole of the detector array affects considerably only the low energy part of the ^{6}Be spectrum at forward and backward angles and has no significant influence on the spectrum shape at $E_T > 2$ MeV in the whole angular range. The maximum in the angular distribution for the population of the 2^+ excited state which mainly corresponds to the $\Delta L = 2$ angular momentum transfer is clearly seen in the region of $\theta_{6Be} = 50^o$–70^o. From figure 1(b) one can see that the maximum of the bump at about 35^o in the c.m. system is well below the maximum of population of the 2^+ state situated at about 60^o. It is natural to suppose that the whole structure is related to the $\Delta L = 1$ angular momentum transfer, populating possible $J^- = \{0^-, 1^-, 2^-\}$ configurations. To extract quantitative information about properties of this phenomenon, the experimental distortions due to the geometry of the detector system and the efficiency of particle registrations have been taken into account.

By simulation based on the developed model [12, 13] and the method [5], the spectrum in figure 1(b) has been reproduced well in the whole energy and angular ranges. Figure 2 shows typical examples of the fits of the experimental spectra measured at 10^o, 60^o and 170^o in the c.m. system of the ^{1}H(^{6}Li,^{6}Be)n reaction. Reasonable fits have been obtained in the whole angular range. With the same set of model parameters we were able to reproduce the measured spectra as a superposition of the three components which correspond to population of the ground 0^+ state, the first excited 2^+ state and negative parity states composing the broad structure with a maximum at about ~14 MeV. The relative contributions of these states to the cross section are estimated to be around 20%, 20% and 60%, respectively [1].

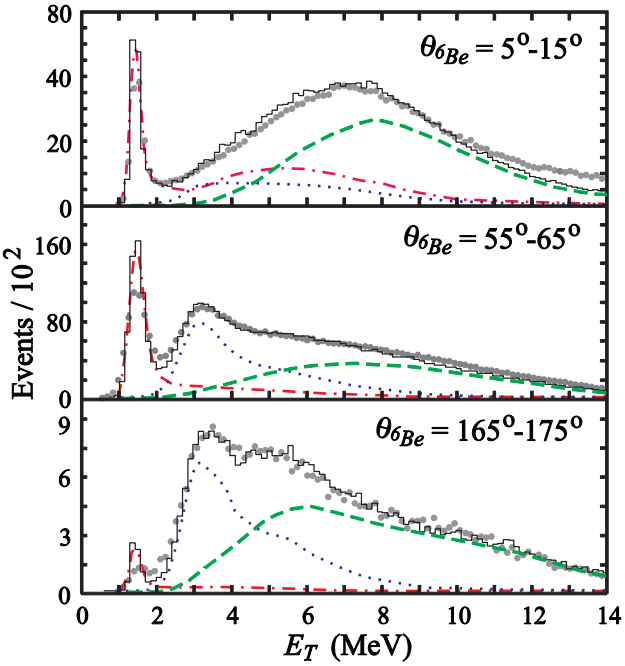

Fig. 2. Examples of projections made on the E_T axis in three angular bins. Grey circles and solid-line histogram show the experimental spectra and their fits. The dash-doted, dotted and dashed lines represent the energy profiles and relative values of contributions coming from the 0^+, 2^+ and J^- states.

2.2 ^{10}He data analysis

Main results of a data analysis obtained for the ^{3}H(^{8}He,p)^{10}He reaction are summarized in the figure 3. The kinetic energy $E(^8\text{He})$ of ^{8}He in the c.m. system of ^{10}He is plotted against E_T in the panel (a). This presentation allows us to estimate background conditions and reject events located outside the kinematically allowed region. Events appearing below the solid line in figure 3 (a) satisfy the condition $E(^8\text{He}) < E_T/5$. To take into account the experimental resolution, we present below the results obtained for events located inside the broader shaded triangle. The background inside the triangle was measured in runs with an empty target and was found to be negligible.

Projected missing-mass spectrum from the data in the panel (a) is shown by points with error bars in figure 3(b). The ^{10}He g.s. peak is clearly seen at about 2.1 MeV. Above the g.s. the spectrum is quite featureless showing a smooth rise of counts above 4 MeV. The $J^\pi = 0^+$ g.s. spectrum of ^{10}He theoretically predicted in Ref. [14] is superimposed on the experimental points in figure 3(b). We take notice of quite good correspondence observed between the experiment and theory within the ^{10}He g.s. peak.

The angular distribution of ^{8}He versus a ^{10}He decay energy is shown in figure 3(c). Three regions with prominent and qualitatively different correlation patterns are notable in this plot: (i) "s-wave" range $E_T < 3.5$ MeV, (ii) "s/p interference" range $4 < E_T < 6$ MeV and (iii) "$s/p/d$ interference" range $6 < E_T < 8$ MeV. The angular distributions for these energy ranges obtained under the condition $\varepsilon = E_{nn}/E_T < 0.5$ (E_{nn} is the n–n relative energy)

are shown in figure 4(a,c,e) together with fits obtained by using the expression

$$w = [AP_0(x) + B\sqrt{3}P_1(x) + C\sqrt{5}P_2(x)]^2 + D^2 \quad (1)$$

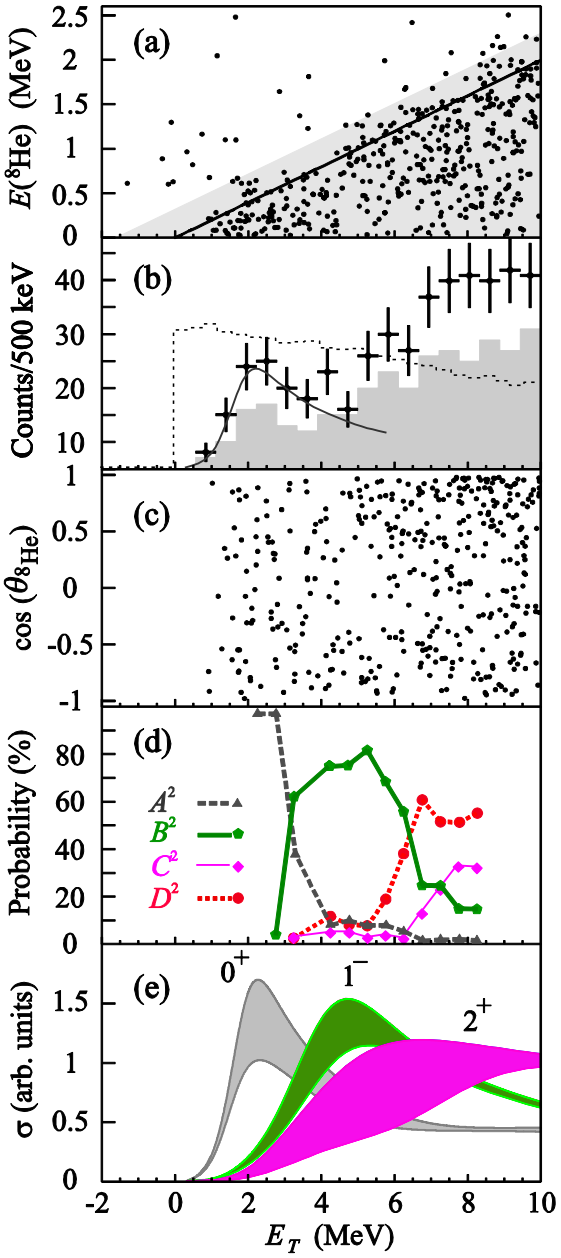

Fig. 3. (a) Scatter plot of $E(^8\mathrm{He})$ vs. E_T. (b) ^{10}He missing mass spectrum. Points with error bars correspond to the total bulk of events, while the grey histogram is obtained under a condition $E_{nn}/E_T < 0.5$. The dotted histogram shows the detection efficiency. The theoretical curve from the panel (e) is given to guide eye. (c) Angular distribution of ^{8}He in the ^{10}He c.m. system. (d) Squared amplitudes of different partial contributions in Eq. (1) deduced from the angular distribution. (e) Theoretically predicted ^{10}He spectra for different J^π values. The shaded areas reflect the uncertainty of these calculations.

Here P_l are Legendre polynomials with $x = \cos(\theta_{^8\mathrm{He}})$. Coefficients A, B and C are the amplitudes of coherent s-, p- and d-wave contributions, respectively, while D takes into account a "background". The energy behavior of these amplitudes is presented in figure 3(d). We used the additional condition $\varepsilon < 0.5$, as in the limiting case $\varepsilon \to 1$ the angle $\theta_{^8\mathrm{He}}$ becomes degenerated. It is also obvious that at ε close to unity, this angle is poorly defined from the data due to errors in the momentum reconstruction.

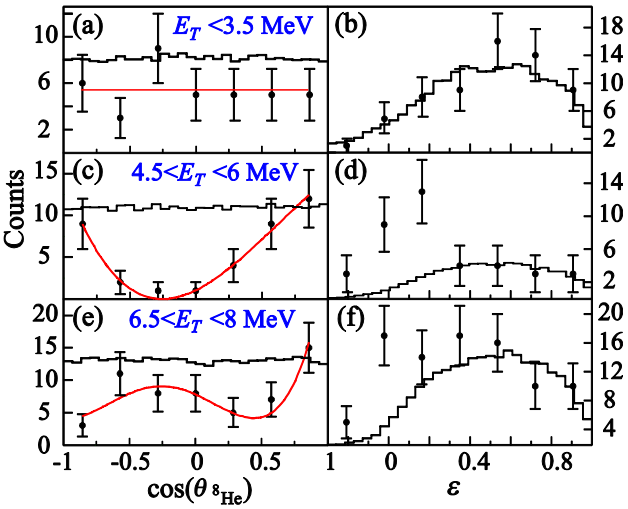

Fig.4. Panels (a,c,e) show angular distributions of ^{8}He measured in different energy ranges of ^{10}He excitation. Solis curves were obtained by using the Eq. (1). Panels (b,d,f) present energy distributions between neutrons obtained for the same energy ranges. Dots with error bars are the experimental data, the histograms show the detection system response for the 4 body (i.e. p+^{8}He+n+n) phase volume.

In the low energy range $E_T < 3.5$ MeV the main contribution comes from g.s. population of ^{10}He with $J^\pi = 0^+$ therefore the angulare distribution shown in figure 4(a) is isotripic one. We take a notice of region $4.5 < E_T < 6$ MeV, see panel (c), where the distribution tends to zero around small values of $\cos(\theta_{^8\mathrm{He}})$ indicating that only *coherent contributions* take place in this energy range. Why there are such expressed correlation patterns for ^{8}He fragment distribution and how they could be connected to the quantum numbers of the whole ^{10}He system? In our analysis we base on experience obtained in the analogous correlation studies of the three-body decay of the ^{5}H system (t+n+n channel) populated in a (t,p) transfer reaction [15,16]. In such three-body systems prominent correlation patterns could be formed if the reaction mechanism is one-step like the direct reaction mechanism and the transferred spin is zero ($\Delta S = 0$). For such conditions the formed correlations could be revealed in the frame where Z axis coincides with the transferred momentum vector, because only zero projections of the orbital momentum are transferred resulting in the population of completely aligned configurations in the final state.

To understand how the alignment of the whole three-body system is converted into the expressed correlation patterns for the selected ^{8}He fragment, one needs to consider the structures of the ^{10}He states. There are two sets of possible major configurations for the ^{10}He wave function with different J^π which interfere with each other, see figure 5. The set with $S = 1$ can be rejected for the following reasons: (i) the transfer of two neutrons in $S = 1$ configuration is very unlikely. Extensive experience gained

in the (t,p) reaction studies points to strong dominance of a "dineutron" ($S = 0$) transfer; (ii) for the 0^+ and 2^+ states the orbital momentum l_y of ^{8}He is coupled with the orbital momentum l_x of two neutrons to the total orbital momentum $L = 1$. Complete alignment of L does not mean any specific alignment of the ^{8}He orbital momentum l_y. In contrast, for the $S = 0$ configurations the $l_x = 0$ dominance is expected and the complete alignment of the total orbital momentum L is directly makes the complete alignment of ^{8}He orbital momentum l_y. In this case the amplitudes for the angular distributions of ^{8}He in the selected ^{10}He c.m. system are obtained as a result of coherent summation of Legendre polynomials $P_l(x)$. This provides the explanation for Eq. (1).

The level ordering 0^+, 1^-, 2^+ is inferred from the configuration choice shown in figure 5(a). Thus, the correlation data provide evidence for anomalous level ordering in ^{10}He. For the 1^- state the proposed correlation analysis gives the energy of about 5 MeV. For the 2^+ state we can establish only energy range where the corresponding set of quantum numbers is important, see figure 3(d).

According to the calculations of Ref. [14] extended to the 1^- and 2^+ excitations of ^{10}He, the expected peak positions and forms were plotted in figure 3(e). The model predictions for the ^{10}He spectrum population give quite broad structures with very asymmetric shapes. The shaded areas show the ranges provided by the theoretical calculations with a realistic parameter variation. The calculation results are very stable for the g.s. energy but demonstrate increasing uncertainty for the higher-lying excitations. However, in all the calculations the lowest excitation is 1^- providing additional support to the proposed experimental spin assignment.

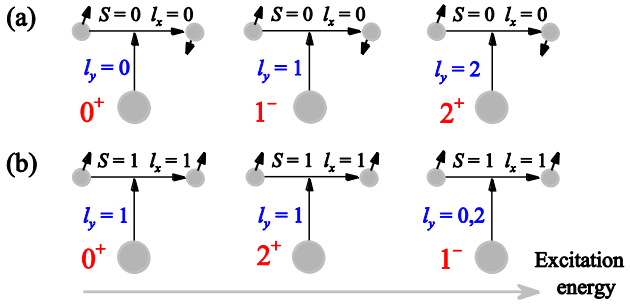

Fig. 5. Expected major components of ^{10}He wave function with different J^π in the cluster ^{8}He+n+n representation. The rows (a) and (b) demonstrate the two sets of components which may interfere in the angular distributions of ^{8}He in the ^{10}He c.m. frame. States with different J^π are arranged by an energy position expected for a particular configuration.

3 Discussion

As it is mentioned above, we focus on a possible nature of the low energy continuum observed in the ^{6}Be spectrum from the ^{1}H(^{6}Li,^{6}Be)n reaction. It deserves a serious attention as a dominating phenomenon responsible for more than 50% of the cross section of population of ^{6}Be states under ~16 MeV. The observed behaviour is not very surprising. Low-energy continuum in charge-exchange reactions has been seen in some previous experiments devoted to studies of light nuclei [17]. The important role of dipole excitation has also been noted in a number of papers. But very often the analysis was confined to fitting the continuum by several broad resonant-like structures and discussions of properties of these resonances. As an example in [18] the continuum part of missing mass spectrum from the ^{6}Li(^{7}Li,^{7}Be)^{6}He reaction was fitted by three gauss-function components, and three broad resonances at 6, 12, and 19 MeV were claimed. The maximum at excitation energy of ~6 MeV with a width of ~5 MeV was treated as due to a "soft-dipole response, expected in nuclei with neutron halo".

In our experiment we have measured not only the energy profile of the ^{6}Be spectrum but a complete set of the kinematic variables. On very high statistical level we see a regular behavior of all variables and do not see the reasons to decompose the continuum at some components. We treat the continuum up to ~16 MeV (at least the most part of the corresponding cross section) as having a unique nature. It could be explained by the excitation of the isovector soft dipole mode.

So, our interpretation is different from the previous interpretations of the low-energy continuum populated in the charge-exchange reactions [18-20] and significantly clarify the situation with the "soft" excitations in $A = 6$ nuclei. It was shown early [1] that our calculations provide very reasonable and consistent description of the three different sets of data: soft dipole mode in ^{6}He and isovector soft dipole mode in ^{6}He and ^{6}Be nuclides.

A definitely established energy of the ^{10}He ground state with $J^\pi = 0^+$ is an important result. Its reliability follows from auspicious features of the two-neutron transfer reactions like ^{3}H(^{8}He,p)^{10}He making it a trusty tool for studies of nuclei with large neutron excess. The shape and energy position of the ^{10}He ground state verify that, just as it is in other nuclei with the magic number of eight neutrons, the six neutrons, available in ^{10}He above the ^{4}He core, take up their positions to complete the 0p shell. This is in accord with the recently obtained energy of the ^{9}He ground-state resonance lying at 2 MeV above the ^{9}He $\rightarrow$ ^{8}He + n decay threshold [21]. Coupling the S = 1/2 spin of the odd (unpaired) neutron with the p-shell orbital momentum $l = 1$ gives a spin-parity of the ^{9}He ground-state resonance $J^\pi = 1/2^-$. The two $J^\pi = 1/2^-$ neutrons in ^{10}He are paired resulting in the ground-state spin-parity $J^\pi = 0^+$. Then an expected pairing energy of about 1.9 MeV comes out for the two last valence neutrons of ^{10}He.

The existence of low-lying 1^- excitations at $E_T \sim 5$ MeV in ^{10}He is not something totally unexpected in the nearby exotic nuclei. Such excitations in the form of a soft dipole mode are known for ^{6}He [22], ^{11}Li [23], and there is an evidence that 1^- is the lowest excitation in ^{8}He spectrum [10].

The importance of the intruder configuration is evident in ^{11}Be where the existence of the neutron halo is connected to the anomalous $1/2^+$ spin-parity of the ground state. In the ^{12}Be spectrum the breakdown of the $N = 8$ shell closure is seen due to the existence of the low-lying 1^- state. The importance of this phenomenon

was broadly discussed both from experimental [24,25] and theoretical points of view [26,27]. Our results provide novel information on the evolution of low-lying level systematics of the $N = 8$ isotones. In ^{10}He the 1^- state is found at the energy comparable to that in ^{12}Be, while the 2^+ state is at the energy comparable to that in the other members of the isotone chain.

4 Conclusion

New results about g.s. and excited states of ^{6}Be and ^{10}He were obtained in the ^{1}H(^{6}Li,^{6}Be)n charge-exchange reaction and ^{3}H(^{8}He,p)^{10}He two-neutron transfer reaction carried out at the ACCULINNA fragment separator. The spectrum up to 16 MeV of energy E_T is completely described by population of three main structures in ^{6}Be: 0^+ at 1.37 MeV, 2^+ at 3.05 MeV and the $\{0^-, 1^-, 2^-\}$ continuum state mixture at ~4−18 MeV. The negative parity continuum could be interpreted as a manifestation of isovector soft dipole mode.

The low-lying spectrum of ^{10}He was studied in the transfer reaction ^{3}H(^{8}He,p)^{10}He. The 0^+ g.s. energy and the width were found to be 2.1(2) MeV and ~2 MeV, respectively. Owing to specific angular correlations the spin-parity assignment is made for low-lying states of ^{10}He. Based on data analysis one could interpret the ^{10}He spectrum as a superposition of the 0^+, 1^- ($E_T \sim 5$ MeV) and 2^+ ($E_T > 6$ MeV) states. The established level sequence shows that ^{10}He is one more dripline nucleus demonstrating the shell structure breakdown.

Acknowledgement

The authors are grateful to Profs Yu.Ts. Oganessian and S.N. Dmitriev for overall support of these experiments. This work was supported by the Russian RFBR 11-02-00657-a grant. L.V. G., S. A. K., A.V. G., and I. A. E. are supported by FAIR-Russia Research Center grant. L.V. G. acknowledges the support by HIC for FAIR research grant, and Russian Ministry of Industry and Science grant NSh-7235.2010.2.

References

1. A. S. Fomichev, *et al.*, Phys. Lett. B **708**, 6 (2012)
2. S. I. Sidorchuk, *et al.*, Phys. Rev. Lett. **108**, 202502 (2012)
3. O. Bochkarev, *et al.*, Sov. J. Nucl. Phys. **55**, 955 (1992)
4. V. I. Goldansky, Nucl. Phys. **19**, 482 (1960)
5. L. V. Grigorenko, *et al.*, Phys. Lett. B **677**, 30 (2009)
6. L. V. Grigorenko, *et al.*, Phys. Rev. C **80,** 034602 (2009)
7. A. A. Korsheninnikov, *et al.*, Phys. Lett. B **326**, 31 (1994)
8. A. N. Ostrowski, *et al.*, Phys. Lett. B **338**, 13 (1999)
9. H. T. Johansson, *et al.*, Nucl. Phys. A **842**, 15 (2010)
10. M. S. Golovkov, *et al.*, Phys. Lett. B **672**, 22 (2009)
11. A. M. Rodin, *et al.*, Nucl. Phys. A **626**, 567c (1997)
12. L. V. Grigorenko, *et al.*, Phys. Rev. C **80,** 034602 (2009)
13. B. Danilin, *et al.*, Phys. Rev. C **43,** 2835 (1991)
14. L. V. Grigorenko and M. V. Zhukov, Phys. Rev. C **77**, 034611 (2008)
15. M. S. Golovkov, *et al.*, Phys. Rev. Lett. **93**, 262501 (2004)
16. M. S. Golovkov, *et al.*, Phys. Rev. C **72**, 064612 (2005)
17. D. Tilley, *et al.*, Nucl. Phys. A **708,** 3 (2002)
18. S. Nakayama, *et al.*, Phys. Rev. Lett. **85,** 262 (2000)
19. T. Nakamura, Eur. Phys. J. A **13,** 33 (2002)
20. X. Yang, *et al.*, Phys. Rev. C **52,** 2535 (1995)
21. M. S. Golovkov, *et al.*, Phys. Rev. C **76**, 021605(R) (2007)
22. T. Aumann, Eur. Phys. J. A **26,** 441 (2005)
23. T. Nakamura, *et al.*, Phys. Rev. Lett. **96**, 252502 (2006)
24. H. Iwasaki, *et al.*, Phys. Lett. B **491**, 8 (2000)
25. S. D. Pain, *et al.*, Phys. Rev. Lett. **96**, 032502 (2006)
26. B. A. Brown, Prog. Part. Nucl. Phys. **47**, 517 (2001)
27. G. Gori, *et al.*, Phys. Rev. C **69**, 041302(R) (2004)